JOURNAL OF AIRCRAFT
Vol. 37, No. 4, July–August 2000

Optimization of Balanced Field Length Performance of Multi-Engine Helicopters

H. G. Visser*
Delft University of Technology, 2600 GB Delft, The Netherlands

The development is described of a balanced field length trajectory optimization approach for a multi-engine helicopter sustaining a single engine failure. Whereas most studies typically focus on a single flight phase, this study is based on a multiphase formulation, in which the rejected takeoff and continued takeoff trajectories are optimized simultaneously, subject to a field length balancing constraint. The advantage of this approach is that, for any given engine failure time, it allows the flight phase where all engines are still operating to be optimized in such a way that the solution represents the best possible compromise between the conflicting requirements set by the rejected takeoff and continued takeoff flight phases. In addition to balanced field length calculations, the optimization of unbalanced rejected takeoff has been addressed. Combined considerations of balanced and unbalanced rejected takeoff give insight in the choice of the critical decision point. The most important result of the overall optimization process is the optimal all-engines-operating takeoff flight path up to the critical decision point. The usefulness of the proposed multiphase optimization approach is demonstrated in a numerical example involving a point-mass model of the UH-60A twin-engine helicopter.

Nomenclature

C_P = power coefficient
C_T = thrust coefficient
C_x, C_z = horizontal and vertical components of thrust coefficient
c_d = mean profile drag coefficient of rotor blades
d = distance along runway
f_e = equivalent flat plate or drag area
f_G = ground effect factor
g = acceleration of gravity
h = helicopter altitude
I_R = rotor polar moment of inertia
K = weight factor control penalty term
K_{ind} = induced-power factor
m = helicopter mass
P_{AEO} = all-engines-operating normal takeoff power
P_{OEI} = maximum one engine inoperative power available
P_{ref} = current power setting
P_s = available shaft power
R = rotor radius
$\bar{U}_c$, $\bar{U}_t$ = normalized flow components at the main rotor
u, w = horizontal and vertical velocity components
u_x, u_z = normalized pseudocontrols
V = airspeed
V_{TOSS} = takeoff safety speed
V_Y = airspeed for best rate of climb
X_{CTO} = total runway length in continued takeoff
X_{RTO} = total runway length in rejected takeoff
x = horizontal displacement
β = thrust vector inclination angle
γ = flight-path angle
η = power efficiency factor
$\bar{v}_i$ = normalized induced velocity
ρ = air density
σ = rotor solidity ratio
τ = normalized time
τ_{fail} = normalized engine failure time
τ_i = normalized terminal time of phase i
τ_P = engine power decay time constant
Ω = rotor angular speed
Ω_0 = nominal rotor speed

Subscripts

max = maximum value
min = minimum value

I. Introduction

THE balanced field length (BFL) performance of a multi-engine helicopter sustaining a failure in one engine depends on various factors, including ambient conditions (such as wind and turbulence), gross weight, and piloting techniques. To be able to deal safely with the event of an inadvertent engine failure, Federal Aviation Administration (FAA) regulations specify that transport helicopters must be certified. Category-A certification, which applies to (large) multi-engine helicopters, stipulates that helicopters should be able to continue their flight with one engine inoperative (OEI).[1] Similar to fixed-wing aircraft, a pilot must continue the takeoff (CTO) if engine failure occurs after the helicopter has passed the critical decision point (CDP), whereas the takeoff needs to be rejected if the engine fails early during the flight, before reaching the CDP. Whether the CTO or the rejected takeoff (RTO) is critical in determining the required field length depends on several factors, most notably the specification of the CDP. In any case, a category-A certificated helicopter must be able to satisfy OEI operation requirements within the available runway field, for any given gross weight. A BFL is obtained when both RTO and CTO require the same runway length.

Reference 2 presents optimal runway takeoff trajectories for a fairly simple point-mass model, representative of the UH-60A Black Hawk helicopter. The main objective of Ref. 2 is to identify the major parameters that influence runway takeoff operations. A flight strategy is developed that provides a proper balance among the three important factors, namely, runway field length, payload capability, and safety. Nonlinear optimal control problems are formulated in Ref. 2 for both the CTO and RTO after a single engine failure, with the aim to minimize the required field length under specified safety constraints and for a given takeoff weight. Both formulations are subject to maximum and minimum rotor speed constraints, along with thrust magnitude and angle constraints. To select a proper CDP, the state variables at the point of engine failure are systematically varied and used as the initial conditions in the optimal CTO and

Received 22 May 1999; presented as Paper 99-4019 at the AIAA Atmospheric Flight Mechanics, Portland, OR, 9–11 August 1999; revision received 9 February 2000; accepted for publication 9 February 2000.

*Lecturer, Faculty of Aerospace Engineering. Senior Member AIAA.

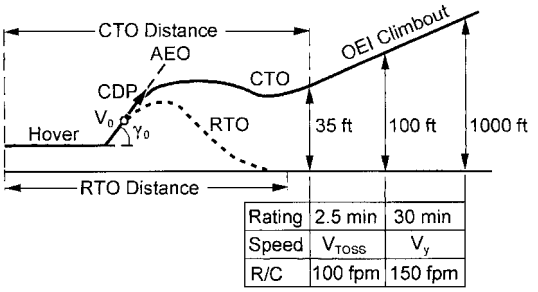

Fig. 1 Category-A helicopter runway takeoff procedure.

RTO trajectory calculations. Based on combined considerations of CTO and RTO, suitable CDPs have been selected to achieve overall minimum runway length.

In Ref. 2 optimization has been restricted to the OEI phase, whereas the phase where all engines are still operating has been based on a simple strategy. Following this strategy, a helicopter would start the takeoff in-ground effect at 5 ft. The helicopter then accelerates horizontally at 0.2 g until $V = V_0$. At V_0, the helicopter starts climbing at a constant airspeed and a constant flight-path angle γ_0 (see Fig. 1). In the follow-on study reported by Zhao et al.,[3] Zhao et al.[2] recognize that the nominal all-engines-operating (AEO) flight path in takeoff plays a crucial role in shaping optimal OEI trajectories and that further studies are needed to determine AEO flight paths that are optimal for OEI flights. The present paper exactly addresses this issue of establishing the best possible AEO flight path up to the CDP.

It is readily clear that the AEO trajectory represents an optimal compromise between conflicting requirements in terms of energy management, set by the CTO and RTO phases. To establish this optimal compromise solution, the AEO, CTO, and RTO flight phases are optimized simultaneously, under the imposition of a field length balancing constraint. More specifically, what we seek to do in this study is to establish the optimal BFL performance as a function of engine failure time. In addition, families of optimal (unbalanced) RTO trajectories, parameterized by the engine failure time, are computed. Based on combined considerations of balanced and unbalanced RTO field length performance, a suitable CDP that provides overall minimum runway length can be extracted. Moreover, the optimal AEO flight path up to the CDP can then be established in the process.

II. Helicopter Modeling

A. Equations of Motion

An augmented two-dimensional point-mass model based on Ref. 3 has been used in the present study. This model is slightly more refined than the model employed in Ref. 2 in the sense that 1) the response of the contingency power available is modeled as a first-order lag, 2) a simple model for ground effect is included, and 3) the time derivatives of the original control variables (thrust vector components) are now used as the (augmented) control variables. The equations of motion presented in Ref. 3 are repeated here in a slightly more generic form, which also allows the representation of the point-mass modeled helicopter in the AEO phase:

$$\dot{h} = -w \tag{1}$$

$$\dot{x} = u \tag{2}$$

$$m\dot{w} = mg - C_z\rho(\Omega R)^2\pi R^2 - \tfrac{1}{2}\rho f_e w\sqrt{u^2 + w^2} \tag{3}$$

$$m\dot{u} = C_x\rho(\Omega R)^2\pi R^2 - \tfrac{1}{2}\rho f_e u\sqrt{u^2 + w^2} \tag{4}$$

$$I_R\Omega\dot{\Omega} = P_s - (1/\eta)C_P\rho(\Omega R)^3\pi R^2 \tag{5}$$

$$\dot{P}_s = (1/\tau_p)(P_{\text{ref}} - P_s) \tag{6}$$

$$\dot{C}_z = u_z \tag{7}$$

$$\dot{C}_x = u_x \tag{8}$$

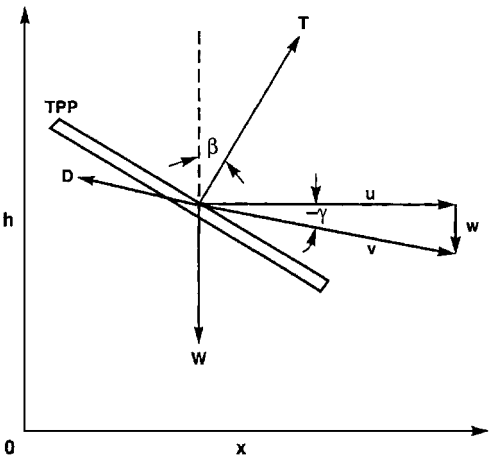

Fig. 2 Point-mass model: forces, speeds, and angles.

A Cartesian reference frame (see Fig. 2) has been used to formulate the force balance equations (3) and (4). The horizontal and vertical components of the thrust coefficient, C_x and C_z, can be readily related to the thrust T and thrust inclination angle β through

$$C_z = C_T\cos\beta \tag{9}$$

$$C_x = C_T\sin\beta \tag{10}$$

where

$$C_T = T/\rho(\Omega R)^2\pi R^2 \tag{11}$$

From Fig. 2, it also follows that airspeed and flight-path angle can be evaluated as

$$V = \sqrt{u^2 + w^2} \tag{12}$$

$$\sin\gamma = w/V \tag{13}$$

The rotor rotational dynamics in Eq. (5) follows from a simple power balance. The required power coefficient C_P is obtained from the following relation:

$$C_P = C_T\sqrt{\tfrac{1}{2}C_T}(K_{\text{ind}}f_G\bar{v}_i + \bar{U}_C) + \tfrac{1}{8}\sigma c_d \tag{14}$$

where

$$\bar{U}_C = \frac{u\sin\beta - w\cos\beta}{\Omega R\sqrt{\tfrac{1}{2}C_T}} \tag{15}$$

$$\bar{U}_t = \frac{u\cos\beta + w\sin\beta}{\Omega R\sqrt{\tfrac{1}{2}C_T}} \tag{16}$$

Equations (15) and (16) represent the two normalized velocity components, perpendicular and parallel to the tip path plane (TPP), that can be used to calculate the normalized rotor-induced velocity,[2,3]

$$\bar{v}_i^4 + 2\bar{U}_C\bar{v}_i^3 + \left(\bar{U}_C^2 + \bar{U}_t^2\right)\bar{v}_i^2 = 1 \tag{17}$$

Note that Eq. (17) is valid outside the vortex-ring state only. In the vortex-ring state an empirical formula has been employed.[2,3] However, in all examined examples, the helicopter stays out of the vortex-ring state. Similar to Ref. 2, a Newton–Raphson scheme has been used to solve Eq. (17).

The term f_G in Eq. (14) accounts for the decrease in induced velocity due to ground effect. To approximate the ground effect in forward flight, a fairly simple model has been used in this study. The model is described in some detail in Ref. 3. A Newton–Raphson solver has been employed for the ground effect model equations as well. Note that in the point-mass equations the center of gravity is assumed to be located at the center of the rotor disk. However, the

model for ground effect takes account of the rotor hub height above the ground.

The dynamic response of the power available is modeled as a first-order lag in Eq. (6). The reference power P_{ref} in Eq. (6) actually depends on the flight phase.

In the AEO phase:

$$P_{\text{ref}} = P_{\text{AEO}} = P_s(0) \tag{18a}$$

and in the OEI phase:

$$P_{\text{ref}} = P_{\text{OEI}} \tag{18b}$$

It is assumed here that the normal AEO takeoff power P_{AEO} and the maximum OEI available power P_{OEI} are constant (control) parameters.

Similar to Ref. 3, the time derivatives of C_z and C_x, rather than C_z and C_x themselves, have been used as the control variables. To this end, the pseudocontrols u_z and u_x have been introduced in Eqs. (7) and (8). By resorting to these pseudocontrols, discontinuities in C_z and C_x at the point of engine failure can be avoided.

In summary, the augmented point-mass dynamic model for flight in a vertical plane is described by eight state variables, h, x, u, w, Ω, P_s, C_z, and C_x, which are governed by two control variables, u_z and u_x, and two control parameters, P_{AEO} and P_{OEI}. Another important parameter is the helicopter mass m. Unfortunately, however, a parametric investigation involving the mass m has not been completed at this stage. Therefore, results for only a single (relatively low) helicopter mass will be presented here.

B. Operational Aspects

Before discussing the mathematical formulation of the BFL trajectory optimization problem for category-A runway takeoff operations, it is instructive to first consider some operational aspects. Notably, the requirements according to FAA Advisory circular AC-29-2A[1] are reviewed to identify the appropriate constraints that must be included in the mathematical problem formulation.

Unlike category-B certified helicopters, category-A certified helicopters are allowed to fly over areas where no emergency landing sites are available. For this reason, a distinction is made between certification for vertical takeoff and landing (VTOL) operations at confined areas and for short takeoff and landing (STOL) from airfields. To be able to perform a safe landing after engine failure, certain combinations of height and forward speed should be avoided. The shape and size of those regions in the (V, h) space will be largely determined by the earlier mentioned parameters related to ambient conditions, gross weight, and piloting procedures. VTOL operations are more critical because of the unsafe low-speed region and may involve considerable weight restrictions for a given helicopter. For this reason it is more practical, not to mention more economical, to make use of STOL procedures whenever possible.

Some typical flight paths for category-A are schematically shown in Fig. 3. If an engine fails before reaching the CDP, the helicopter must land immediately (Fig. 3b). In a safe rejected landing, the helicopter must achieve reasonable touchdown speeds, which implies that constraints on both the vertical and horizontal speed components at touchdown must be included in the trajectory optimization formulation. Because at touchdown the helicopters may still have a forward speed, an additional ground run is required to decelerate to a complete stop. In this study, it is assumed that along the runway the helicopter decelerates at $-0.2\ g$.

The contingency power ratings for category-A are defined in terms of both the level and the duration. Typically, the OEI power ratings include a 2.5- and a 30-min power rating. It is assumed that the 2.5-min OEI power rating is 110% of the AEO maximum takeoff power rating, whereas the 30-min OEI power rating is 105% of the AEO maximum takeoff power rating.

When the engine fails once past the CDP, the takeoff must be completed with the helicopter attaining a minimum altitude of 35 ft and the takeoff safety speed (TOSS) V_{TOSS}, which assures a minimum climb rate of 100 ft/min. During the subsequent OEI climbout phase, the helicopter must be able to satisfy the OEI inoperative

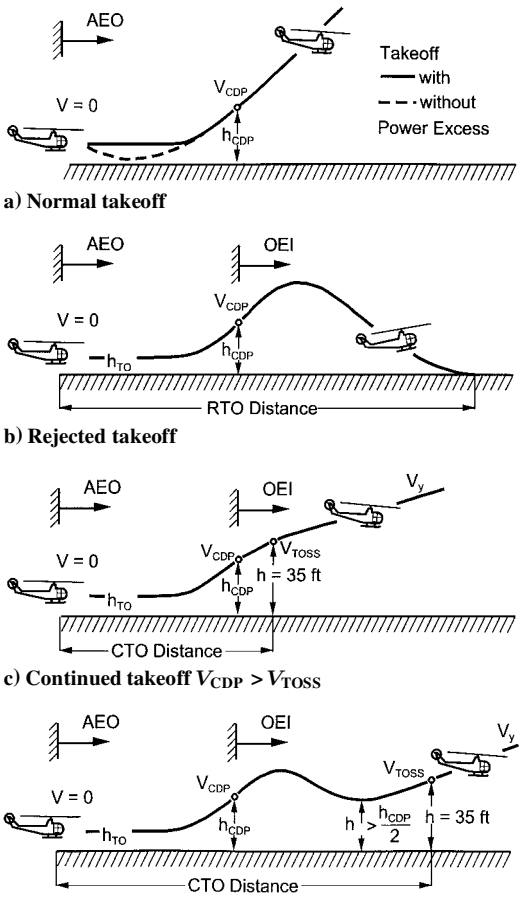

Fig. 3 Typical runway takeoff profiles.

requirements with the remaining power available (Fig. 1). There are actually two segments in the OEI climbout. From 35 ft to at least 100 ft, the helicopter must be able to maintain a minimum rate of climb of 100 ft/min at V_{TOSS} with the 2.5-min OEI power rating. From 100 to 1000 ft/min, the helicopter must be able to accelerate from V_{TOSS} to the airspeed for best rate of climb V_Y with the 30-min OEI power rating. The numerical studies in Ref. 2 bear out that the first segment is more restrictive, and as a consequence, the second segment has been fully disregarded in the current study.

With respect to the selection of V_{TOSS}, it is important to realize that a helicopter requires less power at larger forward speeds, at least below a certain limit. Consequently, V_{TOSS} must be sufficiently high for the helicopter to carry a certain payload in a steady OEI climb. On the other hand, a larger V_{TOSS} leads to a longer CTO runway distance. In Ref. 2, the maximum weight in steady OEI climb has been computed as a function of V_{TOSS}. These results have been used here to select an appropriate V_{TOSS}.

The difference between V_{CDP} and V_{TOSS} has great influence on the optimal trajectory for continued flight (Figs. 3c and 3d). Indeed, if an engine fails at a low speed V_{CDP}, an altitude drop occurs during the continued takeoff. For this reason a minimum altitude constraint according to the requirement shown in Fig. 3d has been included in the optimization formulation; in the CTO phase

$$h > \tfrac{1}{2}h_{\text{CDP}} \tag{19}$$

The strategy for the AEO phase (from hover to engine failure) that has been adopted in Ref. 2 was originally developed for heavily loaded helicopters, that is, helicopters operating with such heavy payloads and in such unfavorable conditions that the available excess power is only sufficient to perform a runway takeoff, not a vertical takeoff.[4] In the employed strategy, preselected values for speed and flight-path angle in the climb are employed which essentially fixes the AEO trajectory in the (V, h) space (Fig. 1). In the present study,

the AEO phase is included in the optimization formulation, and the resulting trajectory is, thus, shaped in the optimization process. It has been assumed here that the helicopter starts from a hover in-ground effect at 5 ft. First, the power required corresponding to this hover condition is calculated. The ensuing AEO phase may then be flown with the power setting at this particular level (no power excess) or with a slightly increased power setting (power excess). In the latter case, obviously it needs to be ensured that the maximum AEO takeoff power rating is not exceeded. Without power excess, altitude may actually drop when accelerating from the hover condition (Fig. 3a). A minimum altitude constraint has, therefore, been included in the AEO phase for safety reasons,

$$h > h_{\min} \tag{20}$$

In this study the minimum altitude $h_{\min}$ has been fairly arbitrarily set at 3 ft.

The aerodynamic and structural limitations of the rotor blades results in constraints on the rotor angular speed, the rotor thrust, and the thrust inclination angle:

$$\Omega_{\min} \leq \Omega \leq \Omega_{\max} \tag{21}$$

$$C_{T\min} \leq C_T \leq C_{T\max} \tag{22}$$

$$\beta_{\min} \leq \beta \leq \beta_{\max} \tag{23}$$

For the AEO phase, a constant rotor rotational speed has been assumed, which is simply arranged by setting in Eq. (21)

$$\Omega_{\min} = \Omega_{\max} = \Omega_0 \tag{24}$$

where Ω_0 is the nominal rotor speed.

C. Physical Parameters UH-60A

In the numerical examples, a model of the Sikorsky UH-60A Black Hawk helicopter has been employed.[2,3,5] This helicopter is powered by two T700-GE-700 turboshaft engines. Some important parameters of this helicopter are presented in the Appendix, along with some parameters used in the trajectory optimization scenarios. In the numerical examples that will be presented only a single mass, corresponding to a relatively lightly loaded helicopter, has been considered ($m = 17{,}715$ lb). The available power P_{AEO} has been set at 2243 hp, which is some 10% above the level required for hover in-ground effect at 5 ft, but well within the maximum takeoff rating.

III. Optimal Control Formulation

A. Variable Scaling

Zhao and Chen[2,3] make use of a scaling procedure for the state and control variables and time and control parameters, to avoid convergence problems in the numerical resolution of the trajectory optimization problems. The same scaling of variables has been adopted in the optimization algorithm employed in the present study. However, because in the presentation of the results the original physical variables are used, a further description of the scaling procedure is omitted here. However, there is one exception that relates to normalized time. Normalized time is defined here as

$$\tau = (\Omega_0/100)t, \qquad \Omega_0 = 27 \text{ rad/s} \tag{25}$$

The primary reason for presenting the results in the form of normalized time histories is that normalized engine failure time τ_{fail} has been used as a control parameter.

B. Multiphase Optimization

As mentioned earlier, to date trajectory optimization studies have primarily aimed at optimizing continued and rejected flight separately, while considering a fixed procedure for the AEO phase, uncoupled from the subsequent phases. Probably the most important reason for synthesizing trajectories from separate flight phases is that the optimization of combined AEO and OEI trajectories is of considerable mathematical and numerical complexity.

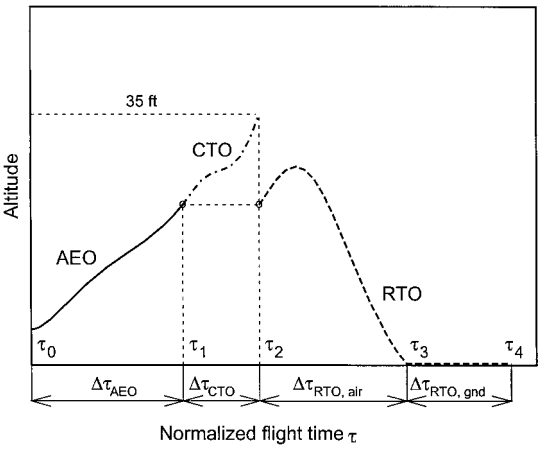

Fig. 4 Multiphase scheme for optimal BFL calculation.

One complication is represented by the event of engine failure; it causes a discontinuity in the dynamic system equations describing the motion of the helicopter. Another complication is that some flight phases are highly constrained, in particular the AEO phase. Indeed, the AEO trajectory should be feasible and practical, while staying outside the restricted region in the (V, h) space. The interior point- and path-type constraints that need to be introduced to overcome the described complications are rather difficult to incorporate in the optimization process, especially when a so-called indirect optimization method[6] is used, such as the sequential gradient restoration algorithm employed by Zhao and Chen.[2,3]

In this study a direct optimization technique has been used that is capable of dealing with the drawbacks already mentioned. In contrast to the indirect approach, a direct approach does not involve solving multipoint boundary-value problems. Rather, the problem of choosing a control function is reduced to choosing a finite set of parameters. Nonlinear programming is then used to select the parameters to minimize a defined objective function. One of the most effective direct numerical methods for path-constrained trajectory optimization is the collocation method.[6,7] Collocation involves discretization of the trajectory dynamics. The discrete dynamics along with the path constraints are then treated as algebraic inequalities to be satisfied by the nonlinear program (implicit integration). More recently, another direct method that uses implicit integration of the system equations has been proposed, namely, differential inclusion.[6,8] Reference 6 recommends that generally preference should be given to the collocation method because the resulting nonlinear programs are typically smaller and easier to solve.

In this study the numerical results have been obtained using both the collocation and differential inclusion techniques. More specifically, the recently developed EZopt (data available online at http://www.ama-inc.com) package has been used to perform the optimal trajectory calculations. This package, which implements both of the described direct optimization methods, proved to be ideally suited for this problem, especially because it turned out to be quite capable in dealing with multiphase optimization problems. In EZopt, discontinuities are possible at phase transitions, as well as different dynamical systems for each phase. These two features are indeed essential for the BFL optimization procedure proposed herein.

Figure 4 shows the multiphase representation used in the present study. The optimization problem is split up into four sequential stages, respectively, the AEO phase, the CTO phase, the airborne phase of the RTO, and the ground run of the RTO. The phase transitions are such that the state variables are continuous, however, with one major exception. The initial state of the airborne RTO phase is directly connected to the terminal state of the AEO phase, and not to terminal state of the CTO. In other words, the CTO and RTO phases have the same initial condition. This implies that, although in the optimization algorithm the four stages are implemented sequentially in time, the CTO and RTO phases are actually concurrently

optimized (the system equations are not explicit functions of time). In the numerical examples, the results will, therefore, be shown with the RTO phase directly connected to the AEO phase.

As far as the time points delimiting the various stages are concerned, only the initial normalized time τ_0 and the normalized engine failure time τ_{fail} $(=\tau_1)$ have an a priori specified fixed value; the remaining staging times are parameters that can be freely optimized.

C. Boundary and Staging Conditions

For the four flight phases defined in Fig. 4, appropriate boundary and staging conditions need to be specified. In general, it is assumed that phase i terminates at the normalized time τ_i^- and begins at time τ_{i-1}^+. The staging conditions are constraints that specify how the state at the end of a particular phase corresponds to the initial state in a subsequent phase. In the multiphase optimization, the following staging conditions have been enforced:

$$\underline{x}\left(\tau_1^+\right) = \underline{x}\left(\tau_1^-\right) \tag{26}$$

$$\underline{x}\left(\tau_2^+\right) = \underline{x}\left(\tau_1^-\right) \tag{27}$$

$$\underline{x}\left(\tau_3^+\right) = \underline{x}\left(\tau_3^-\right) \tag{28}$$

The remaining boundary conditions are specified for each of the four phases separately.

1. AEO Phase

The eight initial conditions for the AEO phase are

$$h(\tau_0) = 5 \text{ ft} \tag{29}$$

$$x(\tau_0) = 0 \tag{30}$$

$$u(\tau_0) = w(\tau_0) = 0 \tag{31}$$

$$\Omega(\tau_0) = \Omega_0 \tag{32}$$

$$P_s(\tau_0) = P_{\text{AEO}} \tag{33}$$

$$\dot{u}(\tau_0) = \dot{w}(\tau_0) = 0 \tag{34}$$

Note that Eqs. (34) represent an implicit specification for the thrust coefficients corresponding to the hover condition.

2. CTO Phase

The terminal constraints for the CTO phase are

$$h\left(\tau_2^-\right) = 35 \text{ ft} \tag{35}$$

$$-w\left(\tau_2^-\right) \geq 100 \text{ ft/min} \tag{36}$$

$$u\left(\tau_2^-\right) \geq u_{\text{TOSS}} \approx V_{\text{TOSS}}(m) \tag{37}$$

$$\dot{u}\left(\tau_2^-\right) = \dot{w}\left(\tau_2^-\right) = 0 \tag{38}$$

$$\dot{\Omega}\left(\tau_2^-\right) = 0 \tag{39}$$

The last three conditions are enforced to ensure a steady-state flight at the end of the CTO.

3. RTO Airborne Phase

The constraints for the RTO phase at touchdown are

$$h\left(\tau_3^-\right) = 0 \tag{40}$$

$$w\left(\tau_3^-\right) \leq w_{\max} \tag{41}$$

$$u\left(\tau_3^-\right) \leq u_{\max} \tag{42}$$

In contrast to Ref. 2, the safe touchdown constraints (41) and (42) are enforced here as inequalities.

4. RTO Ground Phase

The ground phase of the RTO has been integrated in the multiphase optimization process in an analytical form. More specifically, the stopping distance is solved analytically in terms of speed, based on the following trivial boundary condition:

$$u\left(\tau_4^-\right) = 0 \tag{43}$$

D. BFL Performance Index

For the multiphase optimization problem as described, the objective is to minimize the BFL. Total runway length for the complete CTO (including the AEO phase) is simply obtained from

$$X_{\text{CTO}} = x\left(\tau_2^-\right) \tag{44}$$

Similarly, the overall runway length for the complete RTO (up to a full stop) is given by

$$X_{\text{RTO}} = x\left(\tau_4^-\right) = x\left(\tau_3^-\right) + u^2\left(\tau_3^+\right)\Big/0.4\, g \tag{45}$$

Note that the final term in Eq. (45) represents the stopping distance after touchdown. The performance index can be based on either Eq. (44) or Eq. (45), provided that the following field length balancing constraint is taken into account,

$$X_{\text{CTO}} = X_{\text{RTO}} \tag{46}$$

It is recalled that the derivatives of the thrust coefficients are employed as the control variables. The use of these pseudocontrols variables allows the thrust coefficients to be continuous across the phase boundaries and results in a smoother control, partially simulating pilot response delays. No constraints are imposed on the pseudocontrols. However, to avoid unacceptably large control inputs and to smooth the solution further, a quadratic control penalty term has been added to the runway length optimization criterion. The selected performance index is, thus, a weighted combination of the form

$$J = X_{\text{RTO}} + K \int_{\tau_0}^{\tau_3} \left(u_x^2 + u_z^2\right) \mathrm{d}\tau \tag{47}$$

where K is a weight factor. The weight parameter has been selected such that the overall takeoff distance increases by about 10% relative to the case where K has been set to zero (in a typical scenario).

A perhaps more appropriate objective in the optimization problem is to minimize the overall runway length needed, rather than to achieve a BFL. Mathematically, this problem can be stated as

$$\min \max(X_{\text{CTO}}, X_{\text{RTO}}) \tag{48}$$

However, the results in this study demonstrate that this particular objective is achieved by the BFL when both CTO and RTO are equally influential.

E. Unbalanced RTO Flight

The calculation of optimal unbalanced RTO trajectories is much simpler than the optimal BFL calculations because the AEO and CTO flight phases can be completely disregarded. To allow a comparison with optimal balanced RTO trajectories, the initial condition for an unbalanced RTO trajectory is simply the state at engine failure that occurs in a corresponding optimal BFL trajectory. Except for the field length balancing constraint given by Eq. (46), the terminal boundary conditions for the balanced and unbalanced RTO trajectories are also the same.

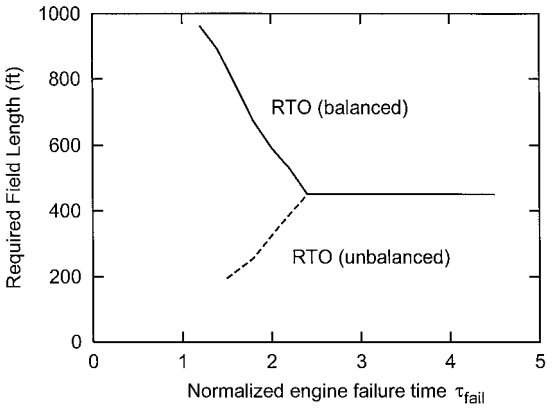

Fig. 5 Required field length as a function of normalized engine failure time τ_{fail}.

IV. Numerical Results

A. CDP Selection

To establish the best possible CDP, the characteristics of optimal BFL trajectories have been examined for a range of values for the normalized engine failure time. Figure 5 shows the optimal BFL as a function of the normalized engine failure time for the example helicopter. Note that in Fig. 5 the optimal BFL results are labeled as RTO (balanced). Figure 5 also presents the results for the corresponding unbalanced optimal RTO trajectories.

Inspection of Fig. 5 shows that initially the BFL dramatically decreases with engine failure time, but that at some point no more progress is made. This observed behavior is fairly easily understood. When an engine fails early during the takeoff, the CTO phase is critical in the BFL computations. As the failure time increases, the required field length for CTO decreases, while the field length required for RTO increases. At about $\tau_{fail} = 2.4$, the RTO and CTO flight are equally influential in determining the BFL. This is reflected by the required field lengths for balanced and unbalanced RTO trajectories being the same at this point. For engine failure times in excess of $\tau_{fail} = 2.4$, the RTO performance is the decisive factor. However, the resulting RTO trajectories will not be significantly different from the trajectory found for $\tau = 2.4$. Indeed, any (normalized) time in excess of $\tau = 2.4$ during which both engines remain operative will be simply absorbed in vertical flight, to avoid an increase in BFL due to reduced RTO field length performance.

Figure 6 serves to illustrate the preceding observations by presenting some more detailed BFL trajectory results for several selected values of the normalized engine failure time. The three selected values for engine failure time represent cases of a fairly early failure ($\tau_{fail} = 1.5$) and a late failure ($\tau_{fail} = 3.5$), relative to the nominal case ($\tau_{fail} = 2.4$).

Figure 6a shows the time histories for speed, whereas Fig. 6b presents the corresponding altitude profiles for the AEO and RTO phases. If an engine fails early during the flight, only a modest energy level has been attained by the helicopter at the point of engine failure, and as a result, both the speed and altitude are relatively low at this point. Figure 6c reveals that due to the power deficiency that results from such an early engine failure, the helicopter is unable to accelerate without trading potential for kinetic energy. Clearly, such a situation is bound to lead to a relatively large CTO distance and, due to the field length balancing constraint, also to a large RTO distance. It can be observed in Fig. 6c that the ground phase of the RTO is actually quite large. This is a direct consequence of the touchdown in the balanced RTO trajectory taking place at the maximum permissible horizontal speed of 40 ft/s (Fig. 6a).

Note that the RTO trajectories that come out of the BFL calculations for engine failure times below $\tau_{fail} = 2.4$ have no practical significance from an operational perspective. Indeed, it is readily clear from Fig. 5 that in the case of early failure a significantly lower RTO distance can be obtained if a strategy is adopted that is based on unbalanced optimal RTO trajectories. The true purpose of

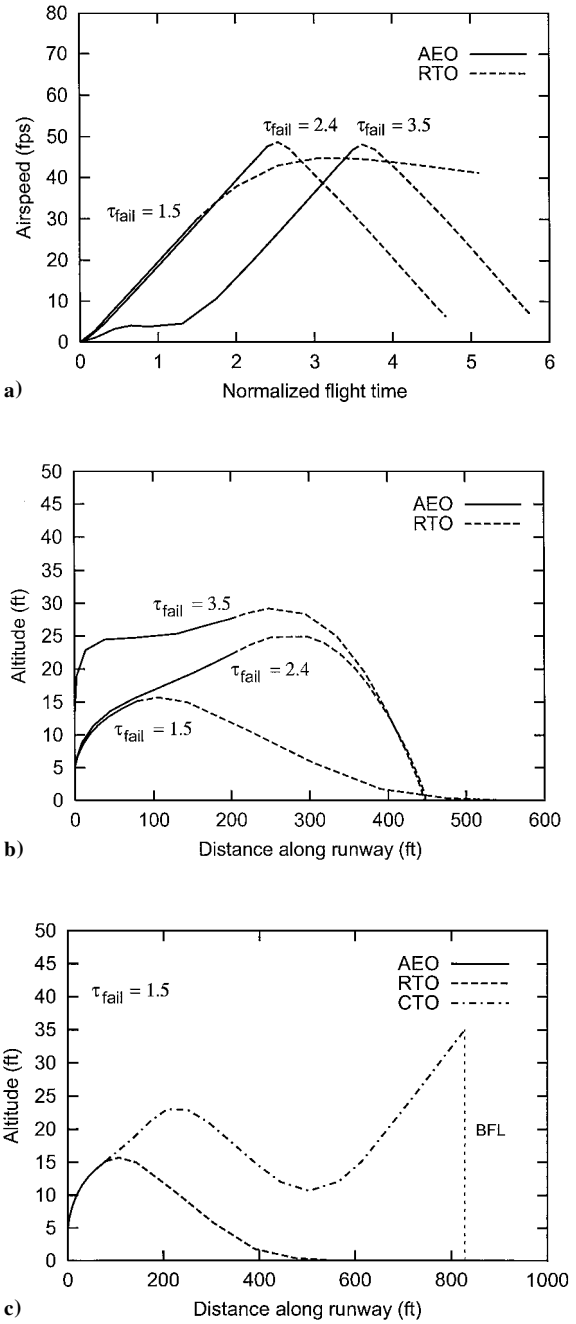

Fig. 6 Optimal BFL trajectories for several values of normalized engine failure time.

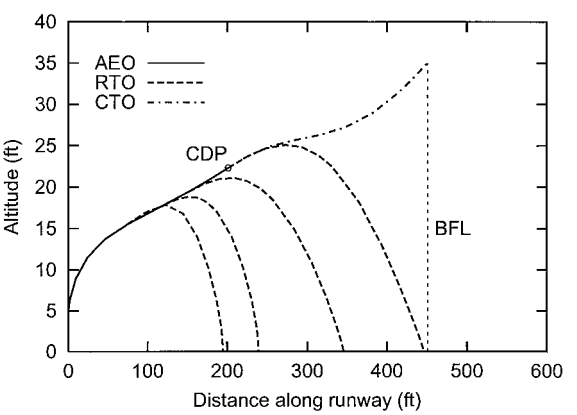

Fig. 7 Several optimal RTO trajectories emanating from the optimal AEO trajectory.

the optimal BFL calculations is to establish the best possible AEO trajectory for a given engine failure time. For early engine failure times, the BFL calculations focus on the optimization of the more restrictive CTO phase, while the RTO requirements assure that the AEO phase ends outside the restricted region in the (V, h) space.

Figure 6b also demonstrates that increasing the engine failure time from $\tau_{\text{fail}} = 2.4$ to 3.5 does not result in a reduction in the required takeoff distance. As a matter of fact, for large engine failure times the resulting RTO trajectories are not all that different. Indeed, the main difference is found in the AEO phase. A close inspection of Fig. 6b makes clear that in the case of a late failure, the helicopter climbs vertically from its initial position. A climb is indeed possible because of the available excess power in the AEO phase.

With respect to the selection of the optimal CDP and the optimal AEO trajectory leading to it, it is readily clear from the preceding observations that the optimal BFL trajectory corresponding to

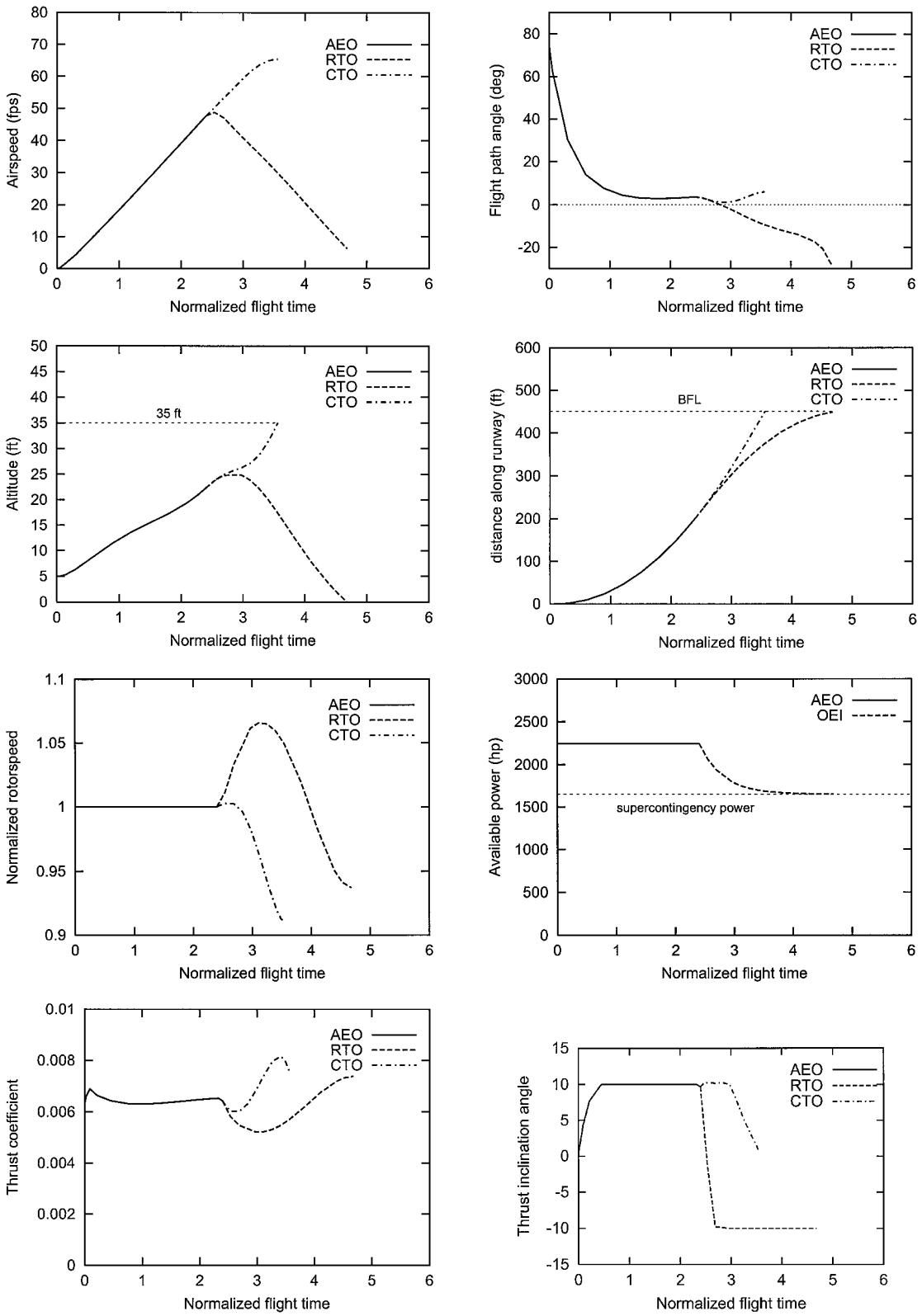

Fig. 8 Optimal BFL solution for normalized engine failure time $\tau_{\text{fail}} = 2.4$.

$\tau_{\text{fail}} = 2.4$ offers the best possible candidate. Figure 7 shows this particular optimal BFL trajectory, along with several optimal unbalanced RTO trajectories that originate at some point on the optimized AEO trajectory. Note that the optimal RTO trajectories shown correspond to the curve labeled RTO (unbalanced) in Fig. 5. From Fig. 7 it can be concluded that the required field length will never exceed the indicated BFL distance, regardless of the point of engine failure.

The main result of the optimization process is that we have now established the best possible takeoff procedure (with respect to the required field length) up to the CDP. Indeed, when the simple AEO strategy of Ref. 2 is replaced with the AEO phase of the optimal BFL solution, a significant reduction in field length can be obtained. The terminal state vector of the optimized AEO trajectory shown in Fig. 7, which will serve as the CDP, includes the following components:

$$V_{\text{CDP}} = 47.65 \text{ ft/s} \qquad h_{\text{CDP}} = 22.28 \text{ ft}$$

$$\gamma_{\text{CDP}} = 3.57 \text{ deg} \qquad x_{\text{CDP}} = 200.98 \text{ ft} \tag{49}$$

It is interesting to actually quantify how much runway reduction can be obtained relative to the simple AEO procedure of Ref. 2, assuming that the CDP is the same. The required runway length for the horizontal acceleration followed by a steady-state climb up to the CDP can be computed from[2]

$$d_{\text{CDP}} = \frac{V_{\text{CDP}}^2}{0.4\,g} + \frac{h_{\text{CDP}} - 5}{\tan \gamma_{\text{CDP}}} \tag{50}$$

Substitution of the terminal values listed in Eq. (49) into the right-hand side of Eq. (50) yields $d_{\text{CDP}} = 453$ ft, which is more than twice the value x_{CDP} found for the optimized BFL.

The optimal AEO performance strongly depends on helicopter gross weight. It is likely that the benefit of optimization will reduce as the gross weight increases.

B. Optimal BFL Trajectory Characteristics

In this section the selected BFL trajectory will be presented in somewhat more detail. Figure 8 presents the time histories for eight state variables for the optimal BFL trajectory corresponding to $\tau_{\text{fail}} = 2.4$. Results are presented for each of the three flight phases, namely, AEO, CTO, and RTO. In the time history for required power, the curve labeled OEI applies to both the RTO and CTO phase. Clearly visible in the time history for the available power is the decay that occurs after engine failure. It is recalled that in the current study it is assumed that the OEI power rating is 110% of the maximum AEO takeoff power rating.

One of the most striking features that can be observed in Fig. 8 is the near-linear behavior of airspeed as a function of normalized flight time for the three respective phases. Note that the touchdown in the RTO trajectory takes place at a relatively low speed (well below the maximum permissible horizontal speed). As a result, the ground phase of the RTO (not shown here) is of a limited extent only. During the final phase of the airborne RTO phase, the rotor energy that has been stored in the initial phase of the RTO is used to develop thrust. This is reflected by the rotor speed first increasing before it subsequently drops to a low value in the RTO trajectory. The thrust vector is tilted backward in the RTO flare. Although the flight-path angle takes on fairly low values in the terminal phase of the RTO, the rate of descent does not violate the imposed boundary constraint at touchdown ($w_{\max} = 3$ ft/s), simply because the airspeed is low in the final phase.

The resulting CTO trajectory does not exhibit any peculiarities either. It is recalled that the terminal boundary conditions for the CTO phase are such that the helicopter reaches the 35-ft screen height in steady state. The screen height is actually reached in a relatively short flight time. In the CTO phase, rotational energy is traded for potential and kinetic energy, resulting in a drop in rotor speed. The horizontal speed that is reached at the 35-ft screen height exactly matches u_{TOSS}, but the climb rate at that point significantly exceeds the minimum requirement of 100 ft/min. By selecting a different value for u_{TOSS}, the climb rate during the OEI climbout can perhaps be reduced, but this requires further investigation.

V. Conclusions

A BFL trajectory optimization approach using a collocation or differential inclusion technique in conjunction with a multiphase procedure has been developed for multi-engine helicopters sustaining a failure in one engine. The essential feature of the proposed approach is that it allows the computation of complete trajectories rather than trajectories synthesized from separate flight phases. Combined considerations of balanced and unbalanced rejected takeoff give insight in the selection of the CDP. The main outcome of the overall BFL optimization process is the optimal AEO takeoff trajectory up to the CDP.

The present study is limited in scope in the sense that an extensive parametric investigation has not taken place yet. Important parameters that need to be examined in future research include takeoff weight, takeoff power rating, initial hover height, and the takeoff safety speed. The current concept is likely to provide a useful basis for conducting such a parametric study. The developed multiphase optimization concept is flexible in the sense that alternative optimization criteria, for example, takeoff weight, additional constraints, for example, a specified field length, or model refinements, for example, a rigid-body model with three degrees of freedom, can be readily introduced.

Appendix: UH-60A Model Parameters

The following presents an overview of some important parameters of the Sikorsky UH-60A Blackhawk helicopter, along with some parameters used in the optimization. The maximum takeoff power is 3086 shaft hp. The considered mass is $m =$ 17,715 lb. The most important rotor parameters are $R = 26.83$ ft, $\sigma = 0.0821$, $\Omega_0 = 27$ rad/s, and $I_R = 7060$ slug ft^2. The thrust constraints used are $C_{T_{\min}} = 0.001$ and $C_{T_{\max}} = 0.01846$. Other values of parameters used in the optimizations include $f_e = 30$ ft^2, $c_d =$ 0.012, $\eta = 0.85$, $K_{\text{ind}} = 1.15$, $w_{\max} = 3$ ft/s, $u_{\max} = 40$ ft/s, $V_{\text{TOSS}} =$ 65 ft/s, $\beta_{\max} = 10$ deg, $\beta_{\min} = -10$ deg, $\Omega_{\max}/\Omega_0 = 107\%$, $\Omega_{\min}/\Omega_0 = 91\%$, $P_{\text{AEO}} = 2243$ hp, and $P_{\text{OEI}} = 1650$ hp.

References

[1] *Certification of Transport Category Rotorcraft*, Federal Aviation Administration, Advisory Circular AC-29A, 1987.

[2] Zhao, Y., and Chen, R. T. N., "Critical Considerations for Helicopters During Runway Takeoffs," *Journal of Aircraft*, Vol. 32, No. 4, 1995, pp. 773–781.

[3] Zhao, Y., and Chen, R. T. N., "Optimal Vertical Takeoff and Landing Helicopter Operation in One Engine Failure," *Journal of Aircraft*, Vol. 33, No. 2, 1996, pp. 337–346.

[4] Schmitz, F. H., "Optimal Takeoff Trajectories for a Heavily Loaded Helicopter," *Journal of Aircraft*, Vol. 8, No. 9, 1971, pp. 717–723.

[5] Prouty, R. W., *Helicopter Performance, Stability, and Control*, Krieger, Malabar, FL, 1990, p. 698.

[6] Conway, B. A., and Larson, K. M., "Collocation Versus Differential Inclusion in Direct Optimization," *Journal of Guidance, Control, and Dynamics*, Vol. 21, No. 5, 1998, pp. 780–785.

[7] Hargraves, C. R., and Paris, S. W., "Direct Trajectory Optimization Using Nonlinear Programming and Collocation," *Journal of Guidance, Control, and Dynamics*, Vol. 10, No. 4, 1987, pp. 338–342.

[8] Seywald, H., "Trajectory Optimization Based on Differential Inclusion," *Journal of Guidance, Control, and Dynamics*, Vol. 17, No. 3, 1994, pp. 480–487.